Growth mechanism of largescale MoS_2 monolayer by sulfurization of MoO_3 film

2016 Mater. Res. Express 3 075009

(http://iopscience.iop.org/2053-1591/3/7/075009)

Materials Research Express

PAPER

Growth mechanism of largescale MoS_2 monolayer by sulfurization of MoO_3 film

RECEIVED
11 April 2016

REVISED
24 June 2016

ACCEPTED FOR PUBLICATION
27 June 2016

PUBLISHED
15 July 2016

Payam Taheri[1,6], Jieqiong Wang[1,2,6], Hui Xing[1], Joel F Destino[3], Mumtaz Murat Arik[1], Chuan Zhao[1], Kaifei Kang[1,2], Brett Blizzard[1], Lijie Zhang[4], Puqin Zhao[5], Shaoming Huang[4], Sen Yang[2], Frank V Bright[3], John Cerne[1] and Hao Zeng[1]

[1] Department of Physics SUNY-Buffalo, Department of Physics, Buffalo, NY 14260, USA
[2] Department of Materials Physics, Xi'an Jiaotong University, School of Science, Xi'an, 710049, People's Republic of China
[3] Department of Chemistry, SUNY-Buffalo, Department of Chemistry, Buffalo, NY 14260, USA
[4] Department of Chemistry, Wenzhou University, Nanomaterials and Chemistry Key Laboratory, Wenzhou, 325035, People's Republic of China
[5] Nanjing Institute of Technology, Nanjing, 211167, People's Republic of China
[6] These authors contribute equally to this work.

E-mail: haozeng@buffalo.edu

Keywords: centimeter-scale MoS_2 monolayer, growth mechanism, photoresponse

Supplementary material for this article is available online

Abstract

Monolayer two-dimensional transition metal dichalcogenides (TMDCs) such as MoS_2 with broken inversion symmetry possesses two degenerate yet inequivalent valleys that can be selectively excited by circularly polarized light. This unique property renders interesting valley physics. The ability to manipulate valley degrees of freedom with light or external field makes them attractive for optoelectronic and spintronic applications. There is great demand for large area monolayer (ML) TMDCs for certain measurements and device applications. Recent reports on large area ML TDMCs focus on chemical vapor deposition growth. In this work, we report a facile approach to grow largescale continuous ML MoS_2 nearly free of overgrowth and voids, by sulfurizing evaporated molybdenum trioxide ultrathin films. Photo conductivity scales with device sizes up to 4.5 mm, suggesting excellent film uniformity. The growth mechanism is found to be vaporization, diffusion, sulfurization and lateral growth, all at local micrometer scale. Our approach provides a new pathway for large-area ML TMDC growth and lithography-free device fabrication.

1. Introduction

Two-dimensional (2D) materials have attracted great attention due to their intriguing physics and potential applications in optics, electronics, optoelectronics and spintronics [1–5]. In the past decades numerous research efforts have focused on graphene, the monolayer (ML) of graphite [6]. Graphene is a gapless semiconductor with its conduction and valance bands meeting at K points in momentum space [7]. The zero band gap results in a small on/off current ratio in field effect transistors, leading to severe restrictions in its applications. To overcome this drawback, there has been enormous effort to develop 2D semiconductors with sizeable band gaps. MLs of two-dimensional transition metal dichalcogenides (TMDCs) such as MoS_2 with an effective honeycomb lattice similar to that of graphene are great candidates for this purpose [8, 9]. While bulk MoS_2 is an indirect bandgap semiconductor, ML MoS_2 has a direct bandgap of 1.8–1.9 eV due to quantum confinement [10]. Further, the broken inversion symmetry creates two inequivalent valleys in the band structure, with inherently coupled valley and spin degrees of freedom. The selective excitation of different valleys by circularly polarized light leads to interesting valley physics and promises applications in spintronics and valleytronics [4, 5, 11–15]. However, the sizes of the exfoliated or grown MoS_2 ML films are sometimes too small for practical use. Demands for large-area MoS_2 MLs have resulted in considerable progress in their synthesis, with techniques such as chemical vapor deposition (CVD) [8, 16–21], vapor–solid (VS) growth [16], sulfurization of predeposited Mo or MoO_3

[8, 16, 22] and thermolysis of Mo compounds [23]. Very recently, essential advances have been made in growing wafer-sized ML MoS_2 with CVD methods [24] and VS methods [16]. Nevertheless, typical challenges in CVD and VS methods are the precise control of the amount of source materials [14, 16] and variation of morphologies at different locations due to spatially-dependent growth parameters. Moreover, the use of excessive oxide source material may lead to oxysulfate impurities [8, 19] according to the Mo–O–S phase diagram [25, 26]. Another popular method to synthesize 2D MoS_2 is by sulfurization of pre-deposited Mo or MoO_3 layers. For example, in a two-step method, thermally evaporated MoO_3 was first reduced by H_2 at 500 °C, and then sulfurized at 1000 °C. Unfortunately, this process yielded isolated domains having 2–3 atomic layers which only became continuous beyond three layers [27]. Another work reported sulfurization of a thin Mo film, which leads to large scale MoS_2 atomic layers [28]. However, the thickness over the entire substrate varied from one to a few layers. In a layer-by-layer sulfurization of MoO_2 microcrystals strategy, rhomboidal shaped MoS_2 with sizes of 10 μm were obtained; however, the thickness is generally larger than ML [29]. Therefore, while sulfurization of pre-deposited precursor layers yields MoS_2 films that are generally more uniform in comparison to those obtained by CVD methods, it is challenging to obtain large scale continuous MLs. Thus, development of a method to grow large area ML MoS_2 that is highly reproducible and with less stringent requirements on growth parameters is highly desirable.

Building upon the earlier advances, we developed a technique to grow cm^2-scale MoS_2 ML by sulfurizing e-beam evaporated ultrathin MoO_3 films on sapphire (0001) substrates. Using this method, the number of MoS_2 layers in films over the entire substrate area can be easily controlled by the MoO_3 precursor layer thickness and sulfurization conditions. Continuous ML films nearly free of voids and overgrowth have been achieved, with film quality comparable to those grown by CVD methods at higher temperatures. For studying the transport properties of ML MoS_2, it is important to eliminate overgrowth because it may completely mask the ML signal. Based on systematic control experiments, we propose a three-stage growth mechanism, where MoO_3 film is vaporized and transported, followed by initial nucleation of single crystal ML islands, and growth and merging of these islands to form a continuous ML film, at the expense of adjacent 3D nanoparticles. Furthermore, *in situ* patterning of ML films can be realized by sulfurization of MoO_3 deposited through evaporation masks, and transport devices can also be fabricated lithography-free. Our technique offers a new pathway to create large-area 2D TMDC materials and devices.

2. Experiment

Growth procedure. Sapphire with *c* orientation ((0001) plane) was consecutively cleaned by acetone/ethanol/DI-water and used as the substrate. Ultrathin MoO_3 films with a nominal thickness of 5–10 Å were deposited on sapphire substrates by electron beam evaporation. The evaporation rate was maintained at 0.1 Å s^{-1}. Pre-deposited MoO_3 films and sulfur (⩾99.95% purity, alfa aesar) were used as Mo and S precursors, respectively. As shown schematically in figure 1(a), the sapphire substrate with MoO_3 film was placed in zone 2 of a 2″ quartz tube furnace; while 4–8 mg of S is located 30 cm upstream in zone 1. The temperatures of both zones were independently controlled, and the temperature ramping profiles of the two zones were coordinated to control the sulfur vapor pressure at the growth temperature of MoS_2 (shown in figure 1(b)). N_2 was used as the carrier gas with a flow rate of 40 standard cubic centimeters per minute at ambient pressure. The growth parameters including the growth temperature, reaction time and carrier gas flow rate were optimized for the synthesis of high quality ML films.

In a typical synthesis, the quartz tube was first kept in N_2 flow for 30 min before ramping up the temperature to remove moisture and air. Sulfur source temperature (zone 1) was then increased to 190 °C at a rate of approximately 6 °C min^{-1}, and heating was turned off after 5 min. The substrate temperature (zone 2) was simultaneously increased to 745 °C at a rate of ~25 °C min^{-1}, with the growth time of 5 min at 750 °C and a subsequent in-furnace natural cooling. The heating profiles for the two zones are shown in figure 1(b). To obtain continuous ML MoS_2, N_2 gas flow was turned off during the cooling step. This is the key to obtain ML MoS_2 nearly free of overgrowth or voids, which will be discussed in detail later.

Single point Raman and photoluminescence (PL) measurements were acquired using a Horiba JY Inc. LabRam HR confocal Raman microscope with 532.06 nm excitation (Laser Quantum), 100× LWD objective (NA = 0.90, Olympus), 600 grooves/mm grating, and a thermoelectrically cooled CCD detector (Andor Technology Inc.). To maintain consistency, all recorded spectra were acquired at 2.3 ± 0.2 mW laser power with 2 s integration times and averaged 3 times. *Raman mapping* were acquired with a 500 nm × 500 nm pixel size. Peak separation at each pixel was obtained by Gaussian fittings of the E^1_{2g} and A_{1g} modes and taking the difference in peak positions.

PL mapping measurements were acquired using an AIST-NT SmartSPM 1000 interfaced to the aforementioned Raman microscope with a 100× LWD objective (Mitutoyo Corp), over a 10 × 10 μm^2 area

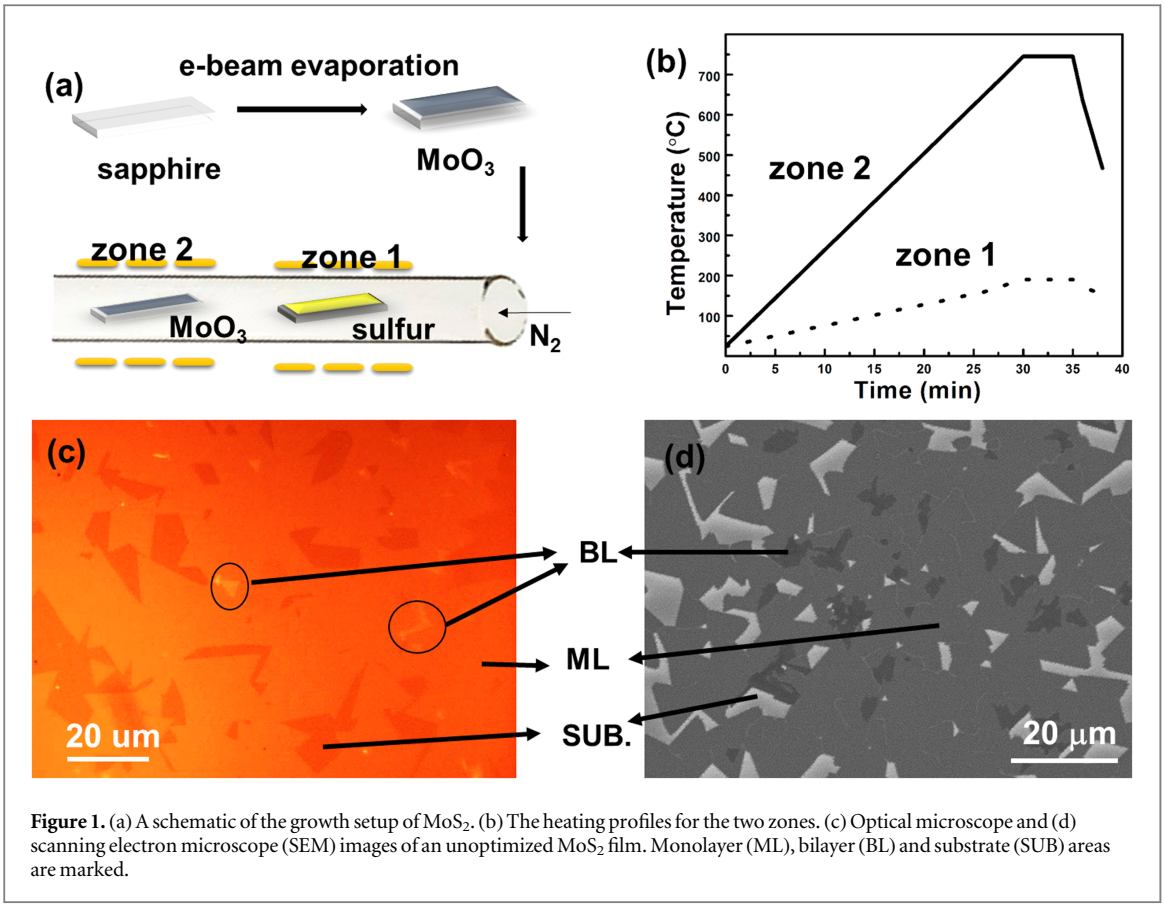

Figure 1. (a) A schematic of the growth setup of MoS_2. (b) The heating profiles for the two zones. (c) Optical microscope and (d) scanning electron microscope (SEM) images of an unoptimized MoS_2 film. Monolayer (ML), bilayer (BL) and substrate (SUB) areas are marked.

with 40 pixel $\times$ 40 pixel spatial resolution. To maintain consistency, all recorded spectra were acquired at 2.3 $\pm$ 0.2 mW laser power with 2 s integration times and averaged 3 times.

Atomic force microscope (AFM) measurements were acquired using an AIST-NT SmartSPM 1000 in intermittent contact mode with an Au-coated Si probe (k = 5.3 N m^{-1}, 130 μm length) (fpN11Au, AIST-NT Inc.) operating at 154 kHz resonant frequency, with a free amplitude of ~20 nm. Images were recorded at 50 $\times$ 50 μm^2 using 512 pixel $\times$ 512 pixel spatial resolution at a scan rate of 1.0 Hz.

Device fabrication and photocurrent measurements. The 5 nm Cr/30 nm Au electrodes were deposited using e-beam evaporation through a shadow mask on a continuous ML MoS_2 sample. Two-terminal devices with varying electrode distances from 125 μm to 4.5 mm were fabricated in parallel without lithography. The photocurrent was measured at a source-drain bias voltage of 1 V, using a Keithley 6487 picoammeter. The light source is a green laser (532 nm) with a spot size of 0.7 mm.

3. Results and discussion

Optical microscope and scanning electron microscope (SEM) images of MoS_2 films are shown in figures 1(c) and (d), respectively. This particular film is essentially ML MoS_2 with bilayer (BL) overgrowth on the top. The purpose of using this unoptimized example is to show that the number of layers can be easily identified from the image contrast. It can also be seen that a well-defined color contrast between MoS_2 and the sapphire substrate is also observed. The high optical absorption in sub-nanometer thick MoS_2 films is one of its unique properties arising from the MoS_2 direct band gap [30]. The brightness/color contrast (see, figure 1(c)) is found to be a good indicator of the number of layers, as was reported in earlier works [10, 16]. As can be seen in figures 1(c) and (d), ML and BL regions can be clearly identified from the optical microscope and SEM images. Such layer identification is further confirmed by Raman and PL spectroscopies. Typical single point Raman spectra are shown in figure 2(a). Two Raman modes, E^1_{2g} and A_{1g}, corresponding to the in-plane vibration of Mo and S atoms and out-of-plane vibration of S atoms, respectively can be clearly seen [9, 17]. The separation between the two peaks is found to be 20.3 $\pm$ 0.5 cm^{-1} in the region identified to be ML MoS_2 by optical and SEM images; while the separation is 22.3 $\pm$ 0.5 cm^{-1} in the regions identified as BLs, consistent with previous work [20]. The corresponding PL spectrum (figure 2(b)) in the ML region exhibits a prominent peak at ~1.87 eV, consistent with the value reported for the direct band gap in ML MoS_2. On the other hand, the intensity of PL in the BL

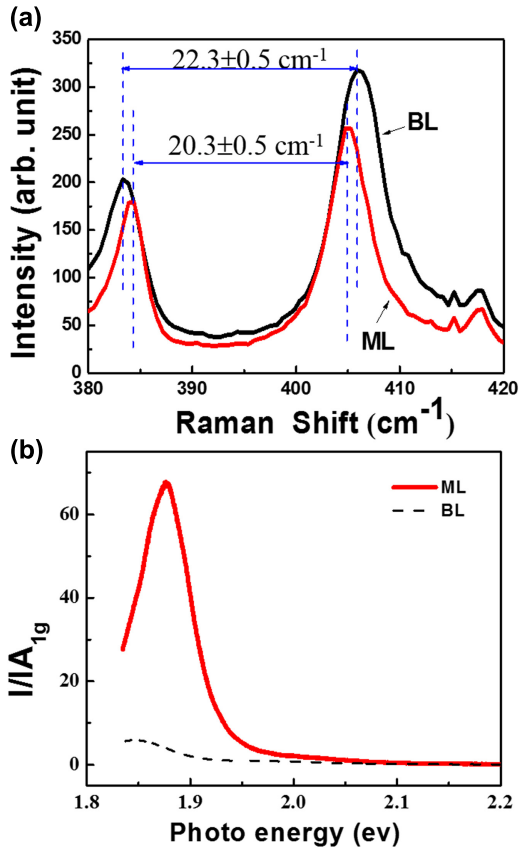

Figure 2. (a) Typical single point Raman spectra of ML and BL MoS_2; (b) PL intensity normalized by the Raman A_{1g} peak intensity as a function of photon energy for ML and BL MoS_2.

region decreases sharply in comparison to the ML region. It has been shown previously that PL intensity depends strongly on the number of layers due to the evolution of interband transition from direct to indirect with increasing layer thickness [10]. PL efficiency, namely, the PL magnitude normalized by the corresponding Raman intensity of the A_{1g} peak, is shown in figure 2(b). As expected, the normalized PL intensity ratio (BL to ML) is <0.1.

The above results show that combining optical and SEM images with Raman and PL spectroscopies are reliable methods to unambiguously discriminate ML from BL MoS_2. These techniques are used in concert to characterize the continuous ML MoS_2 over the entire 1 cm^2 sapphire substrate, obtained by sulfurization of MoO_3 film with optimized growth parameters (*vide infra*). Figure 3(a) presents a typical SEM image of a continuous MoS_2 ML. A gap was intentionally introduced here to show contrast between the sapphire substrate and ML MoS_2. From the SEM image, it is clear that there is virtually no overgrowth or voids, aside from the intentionally introduced gap. A comparison between SEM images of large area ML films with and without overgrowth can be found in Supplementary material (figure S1). All areas within the 1 cm^2 film have been imaged by SEM at different magnifications, and there is no contrast difference other than the intentionally introduced gap and occasional dust particles, suggesting that it is continuous and nearly free of overgrowth or voids. In figure S2, representative SEM images of a ML film at different magnifications are shown, up to an area of 1 mm^2.

The large-area continuous MoS_2 ML film is further confirmed by using Raman spectroscopy to map the peak separation (E^1_{2g} and A_{1g}) across the film in ~100 μm^2 areas across the *entire* 1 cm^2 sample. A typical Raman mapping result is shown in figure 3(b). As seen from the color scale of the mapping, the peak separations range from 19.8 to 20.5 cm^{-1}, consistent with the values expected for ML and considerably smaller than 22.3 cm^{-1} of BL. The average Raman peak separation is 20.3 $\pm$ 0.1 cm^{-1} for all areas mapped (consistent with ML MoS_2). In addition, the AFM line profile measurement across the gap (inset of figure 3(a)) reveals a layer thickness of ~0.65 nm with rms roughness ~0.33 nm (note the sapphire substrate roughness is ~0.3 nm), corresponding to ML MoS_2. A typical AFM image of 50 $\times$ 50 μm^2 area is shown in figure S3. Again, the surface roughness over this area is ~0.33 nm, which is close to the sapphire substrate. On the same sample we also mapped the PL intensities at different locations within 10 $\times$ 10 μm^2 areas. An example is shown in figure 3(c). Typical single point PL spectra for two arbitrary locations within figure 3(c) are shown in figure 3(d). As can be seen there is

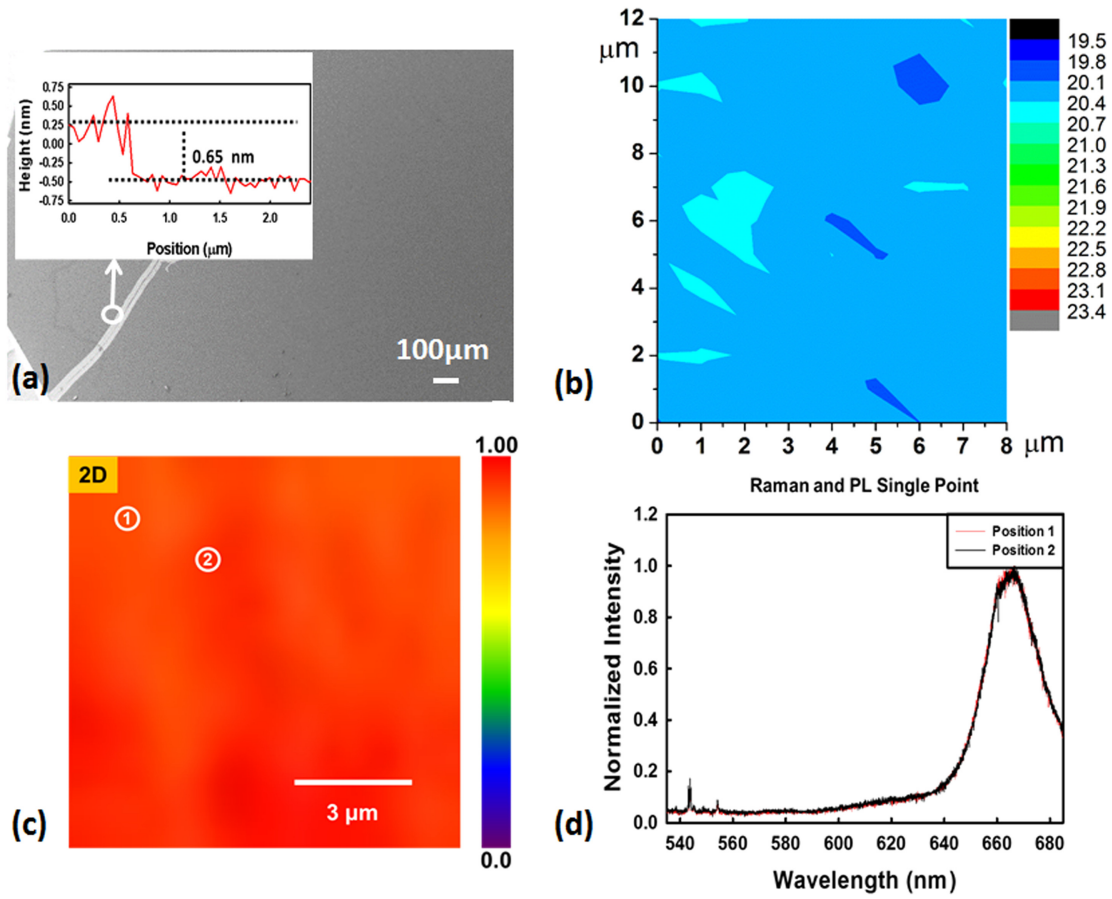

Figure 3. (a) A typical SEM image (inset is the AFM line profile); (b) Raman mapping using separation of E^1_{2g} and A_{1g} peaks (c) PL intensity mapping ($\lambda_{em} = 665$ nm); and (d) PL spectra for two random locations within the PL intensity map, of a continuous ML.

little variation in PL intensity at different points on the ML sample. The variation of PL intensity in the mapped area is smaller than 0.1%. This is an indication of the uniformity of our large area continuous ML sample. It is thus confirmed that a cm^2-scale, continuous ML MoS_2 nearly free of voids and overgrowth has been achieved.

The growth of a cm^2-scale continuous ML MoS_2 film is nontrivial. Previous growth using similar schemes only yielded few-layer MoS_2 and the uniformity is less well-controlled [8]. A few CVD growth studies achieved large-scale ML films through precise control of growth conditions or possible self-limiting growth mechanism [16, 24]. Since CVD inevitably involves initial nucleation (often on defect sites of the substrates) followed by subsequent growth, the morphology is sensitive to variation in substrate morphologies and growth conditions. It is common to observe different morphologies at different locations with slight variation in temperature and gas flow. The advantage of our sulfurization technique as compared to the CVD method is that sulfurization occurs throughout the entire substrate simultaneously, thus uniformity over the whole substrate is improved dramatically. The starting MoO_3 films on the sapphire substrate deposited by e-beam evaporation is either polycrystalline or amorphous. An SEM image (figure S4) shows that pre-deposited MoO_3 film with a nominal thickness of 5 Å is not continuous, but rather consists of densely packed nanoscale islands. The conversion from MoO_3 to ML MoS_2 by sulfurization not only requires S substitution reaction, but also redistribution of Mo atoms. The growth process is a complicated interplay among the crystal growth kinetics, adsorption/desorption and surface diffusion [1]. The low melting temperature and high vapor pressure of the MoO_3 at the optimized growth temperature, coupled with the weak Van der Waals interlayer bonding, is critical for obtaining ML MoS_2 without the need for epitaxial growth and precise controlling of MoO_3 precursor layer thickness down to exactly one ML. In fact, our results suggest that a continuous MoS_2 ML can be obtained with a nominal MoO_3 thickness ranging from 5 to 7 Å. For thicknesses less than 5 Å, significant voids develop while above 7 Å, some overgrowth becomes unavoidable. The key to achieve a continuous ML without significant voids or overgrowth is proper coordination of the sulfur and substrate heating profiles and carrier gas flow, as will be explained below.

Two systematic control experiments were performed to investigate the growth mechanism of continuous MoS_2 ML. These experiments reveal the critical S, MoO_3 and MoS_2 vapor pressure role, which is controlled primarily by temperature and amount of source material. First, the precursor MoO_3 films were patterned

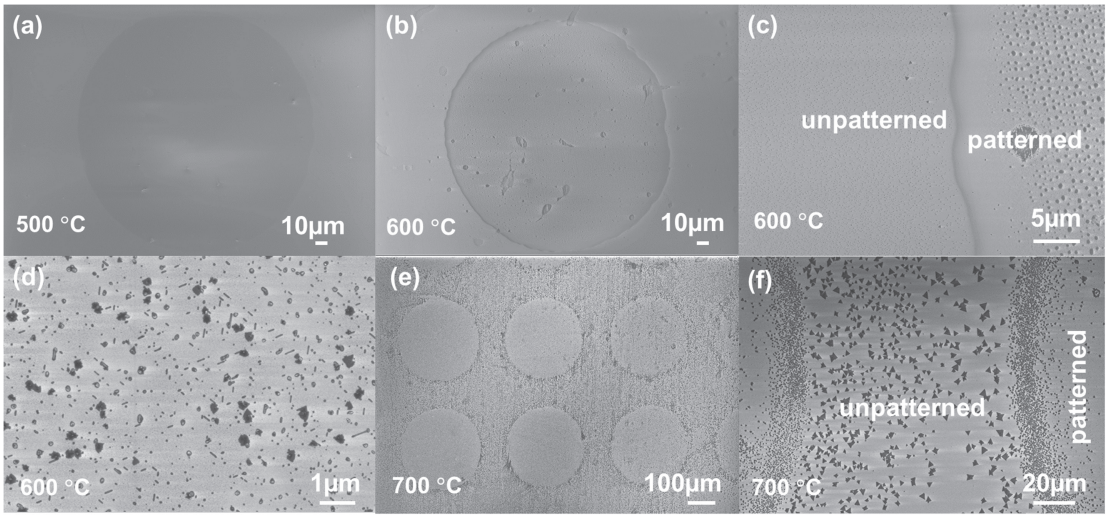

Figure 4. SEM images of patterned MoO_3 sulfurized at different temperatures (a) sulfurized at 500 °C; (b)–(d) sulfurized at 600 °C; (e), (f) sulfurized at 700 °C.

through a shadow mask and sulfurized at different temperatures, to investigate the transport and sulfurization of the Mo source. The samples only stayed at the sulfurization temperature for 1 min and were rapidly cooled by opening the furnace cover to allow the morphologies at the initial growth stage to be retained. The sulfurization temperature is defined as the substrate temperature at which sulfur source temperature reaches 130 °C, when significant sulfur vapor is generated. As can be seen from the SEM images presented in figure 4(a), at sulfurization temperature of 500 °C, the resulting film replicates the original MoO_3 pattern, and no growth in the unpatterned regions has been observed. As the sulfurization temperature is increased to 600 °C (figure 4(b)), while the circular pattern is still visible, there is growth both in and outside the patterned region. The morphologies are different for different regions: in the patterned regions there exist self-assembled islands of a few hundred nm in size, together with smaller 10 nm nanoparticles. Outside the patterns, there exist primarily small nanoparticles (figure 4(c)). Careful examination of these nanoparticles shows that there are two dominant shapes: nanorods and nanoplatelets (figure 4(d)). Considering that the vapor pressure of MoO_3 increases nearly exponentially with increasing temperature, it is plausible that at 500 °C, MoO_3 is not vaporized and sulfurization does not occur, and thus the original MoO_3 patterns are retained. Only at 600 °C is MoO_3 vaporized and transported outside the pattern. The reactivity of MoO_3 with sulfur at this temperature is still low, leading to partial sulfurization. From the crystal symmetry, the nanorods may be predominantly MoO_3 while nanoplatelets may be MoS_2 with sulfur deficiency. Further increasing growth temperature to 700 °C (figures 4(e) and (f)), it is interesting to observe that more material grows outside the patterned region than inside. The grown material consists of mostly discrete triangles of varying sizes from a few hundred nm to 1–2 μm. The spatial distribution of the triangles is uniform and isotropic. Our experiments suggest that MoO_3 can be vaporized, transported over long distances of a few tens of μm, and sulfurized at temperatures of 600 °C, even though bulk MoO_3 has a melting point of 795 °C. Furthermore, the diffusion of Mo is isotropic, and tends to move away from thicker region towards voids on the substrate, consistent with a vapor concentration gradient. This lateral growth mode evens out the local nanoscale thickness variations in the precursor MoO_3 layer, and favors the formation of MoS_2 MLs. This is consistent with the edge growth mode reported by CVD [31], which is due to the high reactivity of MoS_2 edges as compared to the top surface.

In the second control experiment, the amount of sulfur was varied from 4 to 8 mg, in an attempt to influence the MoS_2 morphology. With the same 5 Å thick MoO_3 precursor film, and sulfur mass of 4, 6 or 8 mg, the MoS_2 film morphology changes from mostly discrete triangles and merged triangles (figure 5(a)) to percolating films with many voids (figure 5(b)) and eventually to continuous ML film free of voids or overgrowth (figure 5(c)). Because the melting point of MoO_3 and MoS_2 are 795 °C and 1185 °C, respectively, their vapor pressure differs by many orders of magnitude at the growth temperature of 750 °C. MoO_3 will be rapidly vaporized and sulfurized. However, once sulfurized, MoS_2 evaporation will be drastically reduced. In addition, the amount of sulfur source can determine the sulfur partial pressure, and thus the sulfurization rate; influencing the growth kinetics. Lower sulfur partial pressure cannot lead to complete sulfurization, thus significant amounts of MoO_3 are evaporated, resulting in discrete triangles. Higher sulfur partial pressure, on the other hand, can lead to rapid sulfurization and slow down the evaporation, leading to continuous MoS_2 ML using the optimized growth parameters. Further increasing the sulfur pressure and excess Mo cannot be removed completely from the

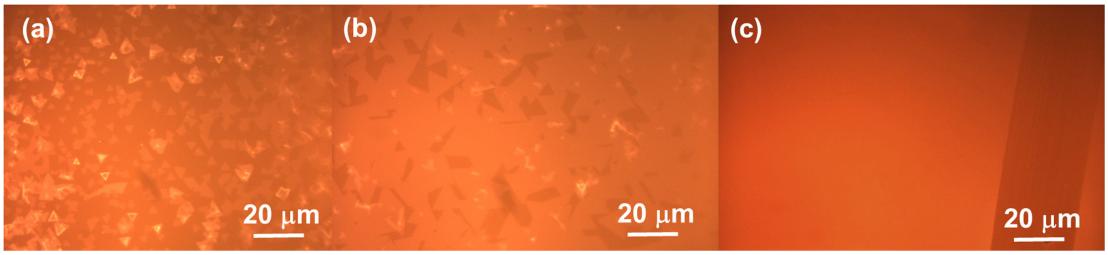

Figure 5. Optical microscope images of MoS_2 monolayer sulfurized with different amount of sulfur (a) 4 mg, (b) 6 mg, and (c) 8 mg.

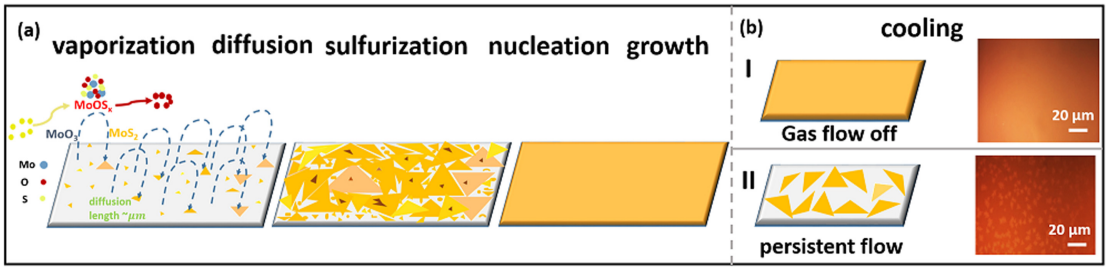

Figure 6. An illustration of the growth mechanism for the large area continuous ML (a) vaporization of MoO_3 and sulfurization to form MoS_2; in this process, the vaporized molybdenum oxides would diffuse tens of μm first, then discrete triangles nucleated, which is followed by growth and merging of the triangles, at the expense of consumption of small nanoparticles, to formation of large area continuous ML; (b) cooling stage for carrier gas flow off (I) and carrier gas flow on (II); figures on right are the corresponding optical microscope images.

substrate, leading to overgrowth on top of the ML MoS_2. It is therefore extremely important to control the sulfur partial pressure during the growth.

Based on the above results, we propose a growth mechanism involving three steps for our optimized growth of ML MoS_2, as shown schematically in figure 6. The first step is the vaporization of MoO_3. This process may be initially aided by the sulfur supply, since sulfur can partially reduce MoO_3 to MoO_2 or lead to formation of molybdenum oxysulfides [29, 32], both of which are volatile species (figure 6(a)). The vaporized molybdenum oxides can then diffuse to regions of substrates with lower molybdenum concentration, namely in the areas not covered by MoO_3, driven by chemical potential difference. Our control experiments show that the diffusion length under our experimental conditions can be tens of μm. This phenomenon helps to even out the local nanoscale morphological variations in the precursor MoO_3 film. That is to say, the precursor film only serves as the local Mo source for uniform growth throughout the substrate; it does not dictate the actual morphology of the final MoS_2. The second step is the sulfurization to form MoS_2, which involves S substitution, reorganization of the lattices and redistribution of materials, shown in figure 6(b). This step leads to uniform nucleation of discrete, single crystal triangular islands of MoS_2 throughout the substrate. The third step is the subsequent growth and merging of these islands to form a continuous MoS_2 ML. Different from CVD growth, in our method all Mo comes from the MoO_3 precursor film. After the initial nucleation of discrete MoS_2 ML triangles, further growth and merging of these ML patterns can only occur at the expense of adjacent numerous small 3D nanoparticles, similar to Oswald ripening in solution phase synthesis [33, 34]. In this step, these 3D nanoparticles vaporize and redeposit at the edges of the discrete triangles. Due to the high triangle density and long diffusion length, these triangles can readily merge, filling the voids in between and eventually form a continuous MoS_2 ML that is nearly free of overgrowth and voids, while the nanoparticles are either consumed or evaporated. Unlike CVD growth, there are no special nucleation sites leading to morphological variations; instead, vapor diffusion and nucleation by sulfurization all take place locally at the micrometer scale, and uniformly across the entire substrate. This ensures that the continuous MoS_2 ML can span the entire substrate. A unique procedure we adopted in our synthesis is to turn off the carrier gas flow during the cooling step. At temperatures of 700 °C and above, MoS_2 has a small but non-zero vapor pressure even though it has a melting temperature of 1185 °C. By turning off the carrier gas flow, the trapped MoS_2 vapor is in equilibrium with the MoS_2 crystals grown on the substrate for longer times, deterring the film from further evaporation. This ensures that a continuous MoS_2 ML can be obtained over the entire substrate (figure 6(c) I). Our control experiment shows that when sulfur is present, ML MoS_2 is partially retained after annealing at 700 °C for 30 min (figure

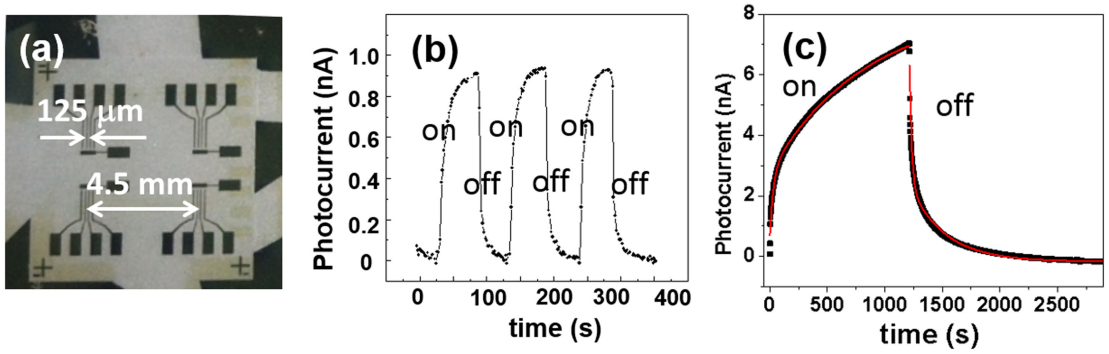

Figure 7. (a) A photograph of the ML MoS_2 devices for photocurrent measurements; distances between electrodes are from 125 μm to 4.5 mm; time-resolved photocurrent at $V_{sd} = 1$ V for devices with channel lengths of (b) 4.5 mm and (c) 125 μm.

S5(b)). On the other hand, if there is persistent N_2 flow during cooling, MoS_2 will be slowly evaporated and continuously carried away. Since there is no additional source supply, the continuous ML is broken into discrete triangular islands as shown in figure 6(c) II. Indeed, our control experiment confirms that ML MoS_2 can be completely evaporated after annealing in N_2 flow at 650 °C for just 5 min (figure S5(c)). This strongly supports the role of sulfur vapor in the growth of continuous ML MoS_2 by sulfurization method. In conventional CVD method when Mo precursor is continuously supplied this is no longer crucial. It should be pointed out that ML films grown by this technique are polycrystalline, consisting of domains with different orientations.

The continuous MoS_2 ML ensures that charge carriers can flow through the entire cm^2-scale sample. We tested for this behavior by using photoresponse measurements on large area ML samples. To measure the photoresponse, we first deposited a 1 cm^2 continuous ML MoS_2, using the method described above; then 5 nm Cr/30 nm Au electrodes were deposited using e-beam evaporation through a shadow mask. Two-terminal devices with varying electrode distances from 125 μm to 4.5 mm were fabricated in parallel without lithography (shown in figure 7(a)). Samples were then illuminated with a green laser (532 nm). The photocurrent was measured at a source-drain bias voltage of 1 V. The dynamics of the photoresponse reflects the presence of trap states in the MoS_2 films [35–38]. To study this, we measured time-resolved photocurrent as the light is turned on and off alternately, for two different channel lengths, as shown in figure 7(b) (4.5 mm) and 7(c) (125 μm), respectively. For the channel length of 4.5 mm the steady state photocurrent is ~0.9 nA, while that for the channel length of 125 μm is ~8 nA. These results show that the detected photocurrent is nearly inversely proportional to channel length, suggesting that the ML is uniform and continuous. To our knowledge, photocurrent on MoS_2 ML with device sizes as large as a few mm have not been reported previously. We further fit the current vs time curve for the 125 μm device and a single exponential model does not fit the data. Instead a double exponential model was used, and two time constants are extracted for the rise and decay parts, respectively. The time constants for the fast component are τ_{rise1} 30 s and τ_{decay1} 825 s, while those for the slow component are $\tau_{rise2} \sim 19$ s and τ_{decay2} 304 s, respectively. The fast and slow components reflect multiple carrier trapping mechanisms, e.g., intrinsic defects in MoS_2, interaction of carriers with the substrate and trapping at the interface between MoS_2 and electrodes. Further experiments are needed to clarify the origins of these different kinetic terms. While more optimization is needed to improve the responsivity and response time for photodetector applications, our results demonstrate that our large area, continuous ML MoS_2 allows fabrication of devices with large sizes or parallel fabrication compatible with conventional semiconductor processing.

4. Conclusion

We have developed a facile method for the growth of cm^2-scale MoS_2 ML films, by sulfurizing e-beam evaporated ultrathin molybdenum trioxide layers. By controlling the MoO_3 layer thickness, amount of sulfur source, and vapor pressure through heating profile, continuous MoS_2 ML films that are free of voids and overgrowth are obtained, eliminating morphological variations over the entire substrate. A mechanism explaining the large-area ML growth is proposed with three stages containing vaporization and diffusion, nucleation and edge growth. Photocurrent profiles were also measured on transport devices fabricated through shadow mask deposition without lithography.

Acknowledgments

Work supported by NSF DMR-1104994, CBET-1510121, DMR-1410599, CHE-0848171, CHE-1126301, CHE-1411435 and MRI-1229208.

References

[1] Butler S Z, Hollen S M, Cao L, Cui Y, Gupta J A, Gutierrez H R, Heinz T F, Hong S S, Huang J and Ismach A F 2013 Progress, challenges, and opportunities in two-dimensional materials beyond graphene *ACS Nano* **7** 2898–926
[2] Gibney E 2015 The super materials that could trump graphene *Nature* **522** 274–6
[3] Novoselov K, Jiang D, Schedin F, Booth T, Khotkevich V, Morozov S and Geim A 2005 Two-dimensional atomic crystals *Proc. Natl Acad. Sci. USA* **102** 10451–3
[4] Scrace T, Tsai Y, Barman B, Schweidenback L, Petrou A, Kioseoglou G, Ozfidan I, Korkusinski M and Hawrylak P 2015 Magnetoluminescence and valley polarized state of a two-dimensional electron gas in WS_2 monolayers *Nat. Nanotechnol.* **10** 603–7
[5] Yang L, Sinitsyn N A, Chen W, Yuan J, Zhang J, Lou J and Crooker S A 2015 Long-lived nanosecond spin relaxation and spin coherence of electrons in monolayer MoS_2 and WS_2 *Nat. Phys.* **11** 830–4
[6] Novoselov K, Geim A K, Morozov S, Jiang D, Katsnelson M, Grigorieva I, Dubonos S and Firsov A 2005 Two-dimensional gas of massless Dirac fermions in graphene *Nature* **438** 197–200
[7] Neto A C, Guinea F, Peres N, Novoselov K S and Geim A K 2009 The electronic properties of graphene *Rev. Mod. Phys.* **81** 109
[8] Lee Y H, Zhang X Q, Zhang W, Chang M T, Lin C T, Chang K D, Yu Y C, Wang J T W, Chang C S and Li L J 2012 Synthesis of large-area MoS_2 atomic layers with chemical vapor deposition *Adv. Mater.* **24** 2320–5
[9] Chhowalla M, Shin H S, Eda G, Li L-J, Loh K P and Zhang H 2013 The chemistry of two-dimensional layered transition metal dichalcogenide nanosheets *Nat. Chem.* **5** 263–75
[10] Splendiani A, Sun L, Zhang Y, Li T, Kim J, Chim C-Y, Galli G and Wang F 2010 Emerging photoluminescence in monolayer MoS_2 *Nano Lett.* **10** 1271–5
[11] Eginligil M, Cao B, Wang Z, Shen X, Cong C, Shang J, Soci C and Yu T 2015 Dichroic spin-valley photocurrent in monolayer molybdenum disulphide *Nat. Commun.* **6** 7636
[12] Srivastava A, Sidler M, Allain A V, Lembke D S, Kis A and Imamoğlu A 2015 Valley Zeeman effect in elementary optical excitations of monolayer WSe2 *Nat. Phys.* **11** 141–7
[13] Riley J, Meevasana W, Bawden L, Asakawa M, Takayama T, Eknapakul T, Kim T, Hoesch M, Mo S-K and Takagi H 2015 Negative electronic compressibility and tunable spin splitting in WSe_2 *Nat. Nanotechnol.* **10** 1043–7
[14] Mak K F, He K, Shan J and Heinz T F 2012 Control of valley polarization in monolayer MoS_2 by optical helicity *Nat. Nanotechnol.* **7** 494–8
[15] Xiao D, Liu G-B, Feng W, Xu X and Yao W 2012 Coupled spin and valley physics in monolayers of MoS_2 and other group-VI dichalcogenides *Phys. Rev. Lett.* **108** 196802
[16] Feng Q, Zhu Y, Hong J, Zhang M, Duan W, Mao N, Wu J, Xu H, Dong F and Lin F 2014 Growth of large-area 2D $MoS_{2(1-x)}Se_{2x}$ semiconductor alloys *Adv. Mater.* **26** 2648–53
[17] Kibsgaard J, Chen Z, Reinecke B N and Jaramillo T F 2012 Engineering the surface structure of MoS_2 to preferentially expose active edge sites for electrocatalysis *Nat. Mater.* **11** 963–9
[18] Lee Y-H, Yu L, Wang H, Fang W, Ling X, Shi Y, Lin C-T, Huang J-K, Chang M-T and Chang C-S 2013 Synthesis and transfer of single-layer transition metal disulfides on diverse surfaces *Nano Lett.* **13** 1852–7
[19] Najmaei S, Liu Z, Zhou W, Zou X, Shi G, Lei S, Yakobson B I, Idrobo J-C, Ajayan P M and Lou J 2013 Vapour phase growth and grain boundary structure of molybdenum disulphide atomic layers *Nat. Mater.* **12** 754–9
[20] van der Zande A M, Huang P Y, Chenet D A, Berkelbach T C, You Y, Lee G-H, Heinz T F, Reichman D R, Muller D A and Hone J C 2013 Grains and grain boundaries in highly crystalline monolayer molybdenum disulphide *Nat. Mater.* **12** 554–61
[21] O'Brien M, McEvoy N, Hallam T, Kim H-Y, Berner N C, Hanlon D, Lee K, Coleman J N and Duesberg G S 2014 Transition metal dichalcogenide growth via close proximity precursor supply *Sci. Rep.* **4** 7374
[22] Orofeo C M, Suzuki S, Sekine Y and Hibino H 2014 Scalable synthesis of layer-controlled WS_2 and MoS_2 sheets by sulfurization of thin metal films *Appl. Phys. Lett.* **105** 083112
[23] Liu K-K, Zhang W, Lee Y-H, Lin Y-C, Chang M-T, Su C-Y, Chang C-S, Li H, Shi Y and Zhang H 2012 Growth of large-area and highly crystalline MoS_2 thin layers on insulating substrates *Nano Lett.* **12** 1538–44
[24] Ji Q, Zhang Y, Gao T, Zhang Y, Ma D, Liu M, Chen Y, Qiao X, Tan P-H and Kan M 2013 Epitaxial monolayer MoS_2 on mica with novel photoluminescence *Nano Lett.* **13** 3870–7
[25] Feldman Y, Wasserman E, Srolovitz D and Tenne R 1995 High-rate, gas-phase growth of MoS_2 nested inorganic fullerenes and nanotubes *Science* **267** 222–5
[26] Liu H, Wong S and Chi D 2015 CVD growth of MoS_2-based two-dimensional materials *Chem. Vapor Depos.* **21** 241–59
[27] Lin Y-C, Zhang W, Huang J-K, Liu K-K, Lee Y-H, Liang C-T, Chu C-W and Li L-J 2012 Wafer-scale MoS_2 thin layers prepared by MoO_3 sulfurization *Nanoscale* **4** 6637–41
[28] Zhan Y, Liu Z, Najmaei S, Ajayan P M and Lou J 2012 Large-area vapor-phase growth and characterization of MoS_2 atomic layers on a SiO_2 substrate *Small* **8** 966–71
[29] Wang X, Feng H, Wu Y and Jiao L 2013 Controlled synthesis of highly crystalline MoS_2 flakes by chemical vapor deposition *J. Am. Chem. Soc.* **135** 5304–7
[30] Zhang H, Ma Y, Wan Y, Rong X, Xie Z, Wang W and Dai L 2015 Measuring the refractive index of highly crystalline monolayer MoS_2 with high confidence *Sci. Rep.* **5** 8440
[31] Zhang Z and Lagally M G 1997 Atomistic processes in the early stages of thin-film growth *Science* **276** 377–83
[32] Kim I S, Sangwan V K, Jariwala D, Wood J D, Park S, Chen K-S, Shi F, Ruiz-Zepeda F, Ponce A and Jose-Yacaman M 2014 Influence of stoichiometry on the optical and electrical properties of chemical vapor deposition derived MoS_2 *ACS Nano* **8** 10551–8
[33] Murray C B, Sun S, Gaschler W, Doyle H, Betley T A and Kagan C R 2001 Colloidal synthesis of nanocrystals and nanocrystal superlattices *IBM J. Res. Dev.* **45** 47–56
[34] Hines M A and Scholes G D 2003 Colloidal PbS nanocrystals with size-tunable near-infrared emission: observation of post-synthesis self-narrowing of the particle size distribution *Adv. Mater.* **15** 1844–9

[35] Liu H, Neal A T and Ye P D 2012 Channel length scaling of MoS_2 MOSFETs *Acs Nano* **6** 8563–9
[36] Yin Z, Li H, Li H, Jiang L, Shi Y, Sun Y, Lu G, Zhang Q, Chen X and Zhang H 2011 Single-layer MoS_2 phototransistors *ACS Nano* **6** 74–80
[37] Lopez-Sanchez O, Lembke D, Kayci M, Radenovic A and Kis A 2013 Ultrasensitive photodetectors based on monolayer MoS_2 *Nat. Nanotechnol.* **8** 497–501
[38] Dumcenco D, Ovchinnikov D, Marinov K, Lazic P, Gibertini M, Marzari N, Sanchez O L, Kung Y-C, Krasnozhon D and Chen M-W 2015 Large-area epitaxial monolayer MoS_2 *ACS Nano* **9** 4611–20